

A quantum trajectory analysis of singular wave functions

Angel S. Sanz,¹ Luis L. Sánchez-Soto,^{1,2} and Andrea Aiello²

¹Departamento de Óptica, Facultad de Física, Universidad Complutense, 28040 Madrid, Spain

²Max-Planck-Institut für die Physik des Lichts, 91058 Erlangen, Germany

(Dated: February 1, 2023)

The Schrödinger equation admits smooth and finite solutions that spontaneously evolve into a singularity, even for a free particle. This blowup is generally ascribed to the intrinsic dispersive character of the associated time evolution. We resort to the notion of quantum trajectories to reinterpret this singular behavior. We show that the blowup can be directly related to local phase variations, which generate an underlying velocity field responsible for driving the quantum flux toward the singular region.

I. INTRODUCTION

The Schrödinger equation is, perhaps, the prototype of a dispersive equation; that is, if no boundary conditions are imposed, its wave solutions spread out in space as they evolve in time [1]. A frequent way to quantify this dispersion is by the so-called dispersive estimates, a topic with a long history [2–4] and whose main goal is to establish tight bounds on the decay of the solutions.

Recently, it has been pointed out that the Schrödinger equation, even for a free particle, presents dispersive singularities [5, 6]: an initial square-integrable profile $\psi(x, 0)$ could result in a solution $\psi(x, t)$ that blows up in a finite time. In the remainder such profiles will be termed as *singular wave packets*. While this singular behavior (sometimes denoted as self-focusing or wave collapse) is well understood in presence of nonlinearities [7–9], it is, at first sight, surprising in a pure linear evolution.

From a mathematical viewpoint, this dispersive blowup can be related to the fact that the linear Schrödinger equation is ill-posed in the space L^∞ : the free propagator is not a Fourier multiplier in L^∞ [10]. In physical terms, dispersive blowup is a focusing phenomenon due to both the unbounded domain of the problem and the propensity of the dispersion relation to propagating energy at different speeds. Interestingly, the same singular behavior has been described in for paraxial beams [11–13], which is consequent with the complete equivalence between the time-dependent Schrödinger equation and the paraxial wave equation [14].

In this paper, we address the physical interpretation of these singularities from the perspective of quantum trajectories. In this picture, quantum formalism is reinterpreted as describing particles following definite trajectories, each with a precisely defined position at each instant in time. However, in this approach, called Bohmian mechanics [15–17], the trajectories of the particles are quite different from those of classical particles because they are guided by the wave function [18–21]. Our analysis shows that the blowup can be directly related to local phase variations, which generate an underlying velocity field (the phase gradient) responsible for driving the quantum flux toward the singular region. To shed light on this point, we compare the blowup with the focusing of a Gaussian and a rectangular wave packet: this demonstrates that imploding solutions are distinguished by an initial phase factor.

Furthermore, for Gaussian wave packets, which can be

nicely analyzed in closed form, it is also observed that there are two types of solutions with very different properties, despite their initial density distributions being identical. One of such solutions leads to a classical type of propagation because the phase factor plays a minor role (or even no role at all). In contradistinction, the other type of solution is characterized by wide initial wave functions with an intrinsic highly oscillatory behavior. This emphasizes the prominent role of the phase as an active agent in the subsequent dynamics.

This article is organized as follows. In Sec. II we briefly discuss the spontaneous generation of a singularity in the Schrödinger equation and introduce the basic elements needed to define a quantum trajectory. In terms of this notion, we analyze the singularity and put forward the fundamental role played by the quantum phase to understand that phenomenon. In Sec. III we examine the behavior of a Gaussian and a rectangular packet and compare with the previous singular wave. Finally, Sec. IV summarizes our conclusions.

II. DISPERSIVE BLOWUP IN THE SCHRÖDINGER EQUATION

A. Spontaneous generation of a singularity

We first set the stage for our discussion. We will be considering the simplest case of the Schrödinger equation for a free particle of mass m in one dimension

$$i\hbar \frac{\partial \psi(x, t)}{\partial t} = -\frac{\hbar^2}{2m} \frac{\partial^2 \psi(x, t)}{\partial x^2}, \quad (1)$$

with the initial Cauchy problem $\psi(x, 0) \in L^2(\mathbb{R})$. The unique solution of (1) can be written in terms of the free-space propagator as [22]

$$\psi(x, t) = \sqrt{\frac{m}{2\pi i \hbar t}} \int_{\mathbb{R}} \exp \left[\frac{im}{2\hbar t} (x - x')^2 \right] \psi(x', 0) dx', \quad (2)$$

where the integral has to be understood in the improper Riemann sense. In this way, the Schrödinger equation appears as an integral equation, rather than a differential one, with the advantage of being valid even if the wave function is not a differentiable function.

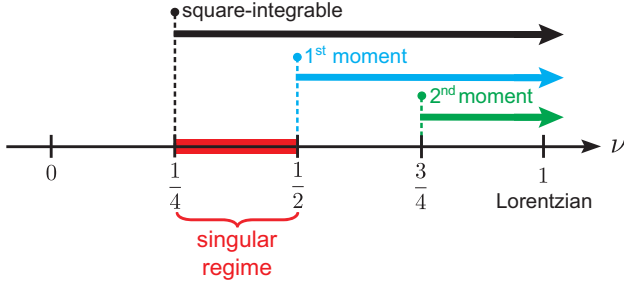


FIG. 1. For $\nu > 1/4$ the wave function (3) is square integrable. The red band indicates the range $1/4 < \nu < 1/2$ where the corresponding $\psi(x, t)$ exhibits a singularity at time $t = \tau$. For $\nu > 1/2$, the corresponding $\psi(x, t)$ is finite everywhere and the first moment $\langle x \rangle$ of the associated probability density $|\psi(x, t)|^2$ exists and it is equal to 0. Finally, the second moment $\langle x^2 \rangle$ is finite for $\nu > 3/4$. The case $\nu = 1$ corresponds to the Lorentzian function.

Slightly generalizing results from Peres [5], we choose the initial data to be

$$\psi(x, 0) = \frac{1}{\sqrt{N_\nu}} \frac{\exp(-\frac{im}{2\hbar\tau}x^2)}{\left(1 + \frac{x^2}{\sigma^2}\right)^\nu}, \quad (3)$$

where N_ν is a normalization constant, and τ and σ are real numbers fixing the time scale and the width of the distribution, respectively. One can check that for $\nu > 1/4$, this function is in the space $L^2(\mathbb{R})$, and so it is a physically admissible solution. When this holds true, the normalization constant is finite and equal to $N_\nu = \sqrt{\pi}\sigma\Gamma(2\nu - 1/2)/\Gamma(2\nu)$.

For $t \neq \tau$, we can apply the Riemann-Lebesgue lemma [23] to show that the resulting $\psi(x, t)$ is continuous in x and t and tends to zero as $|x| \rightarrow \infty$ (although not necessarily uniformly with respect to t). However, at $t = \tau$ a discontinuity occurs: at this time the wave function reads

$$\psi(x, \tau) = \sqrt{\frac{m}{2\pi i \hbar N_\nu}} e^{\frac{im}{2\hbar\tau}x^2} \int_{\mathbb{R}} \frac{e^{-i\frac{m}{\hbar\tau}xx'}}{(1 + x'^2/\sigma^2)^\nu} dx'. \quad (4)$$

This integral is the Fourier transform of a Bessel potential [24] and can thus be expressed as

$$\psi(x, \tau) = \sqrt{\frac{m\sigma^2}{i\hbar N_\nu}} \frac{e^{\frac{im}{2\hbar\tau}x^2}}{2^{\nu-1}\Gamma(\nu)} \left(\frac{m\sigma}{\hbar\tau}|x|\right)^{\nu-\frac{1}{2}} K_{\nu-\frac{1}{2}}\left(\frac{m\sigma}{\hbar\tau}|x|\right), \quad (5)$$

which is valid for $\nu > 0$. Here, K_ν denotes the modified Bessel function of order ν [25], which is infinite at the origin but is nevertheless square integrable. The function $\psi(x, \tau)$ is thus continuous, except perhaps at $x = 0$. To check the behavior around that point, we use the approximation of K_ν for small values of the argument. This leads

$$|z|^{\nu-\frac{1}{2}} K_{\nu-\frac{1}{2}}(|z|) \approx \frac{\Gamma\left(\nu - \frac{1}{2}\right)}{2^{\frac{3}{2}-\nu}} + \frac{1}{|z|^{1-2\nu}} \frac{\Gamma\left(\frac{1}{2} - \nu\right)}{2^{\nu-\frac{1}{2}}} + O(|z|^{2\nu+1}), \quad (6)$$

which shows that the singularity in $\psi(x, \tau)$ thus arises for $\nu < 1/2$. In summary, when

$$\frac{1}{4} < \nu < \frac{1}{2} \quad (7)$$

we get the aforementioned singularity.

A similar analysis can be performed with the moments of the associated probability density $|\psi(x, t)|^2$ [11]. The first moment $\langle x \rangle$ is finite and equal to zero when $\nu > 1/2$, whereas the second moment $\langle x^2 \rangle$ exists provided that $\nu > 3/4$. All this relevant information is concisely summarized in Fig. 1.

B. Quantum trajectories at the singularity

To explore the physical meaning of the singularity and, more particularly, its dynamical emergence, we resort to the concept of quantum trajectory. Apart from providing us with information on the probability density distribution, the wave function $\psi(x, t)$ also contains dynamical information relevant to understand its time evolution. The Bohmian picture stresses this latter aspect, which manifests as quantum trajectories, which are in compliance with the evolution of the quantum flux [21]. To this end, one first decomposes $\psi(x, t)$ as $\psi(x, t) = \sqrt{\varrho(x, t)} \exp[iS(x, t)]/\hbar$, which allows us to split up the density information from the phase information encoded in the wave function. Quantum trajectories are directly related to the local variations undergone by the phase term, $S(x, t)$, according to the so-called Bohmian guiding condition (or local velocity field) [26],

$$\dot{x} = \frac{J(x, t)}{\varrho(x, t)} = \frac{1}{m} \operatorname{Re} \left(\frac{\hat{p}\psi}{\psi} \right) = \frac{1}{m} \frac{\partial S(x, t)}{\partial x}, \quad (8)$$

with $\hat{p} = -i\hbar\partial/\partial x$ being the usual momentum operator in the position representation and $J(x, t)$ the probability current density or quantum flux [27]. We stress that Eq. (8) constitutes a general result that goes beyond any particular interpretation, as it involves quantities that are well defined in any picture of quantum mechanics.

More importantly, Eq. (8) explicitly shows the important role played by the phase, not as an indirect effect (e.g., in the appearance of interference features), but as a fundamental quantity that specifies the local dynamics exhibited by the quantum system on each point of the configuration space at each time. This action emerges in the form of the local velocity field that governs the dynamical evolution of the probability density at any time, making it to move from a region to another, to spread out all over the place, or, as it is the case here, to coalesce on a highly localized region at a very precise time.

After all, note that the above local velocity field is what allows us to establish the connection between the probability density, $\varrho(x, t)$, and the quantum flux, $J(x, t)$, according to the well-known transport relation $J(x, t) = v(x, t)\varrho(x, t)$. Quantum trajectories simply arise after assuming that $v(x, t)$ defines an equation of motion that can be integrated in time, rendering as a result such trajectories. Physically, these trajectories describe the flow of probability at a more local level than the

probability density itself does (to some extent, we can say that this latter quantity provides us with a global view of what is going on). A more detailed discussion on the issue can be found in Ref. [28].

For definiteness, we take the initial state (3), with $\nu = 1/3$, to ensure a singular wave packet. However, to produce a numerically reliable (and physically more realistic) wave function, instead of the initial ansatz (3), we consider the following modified one

$$\psi(x, 0) = \frac{1}{\sqrt{N_\nu}} \frac{\exp\left(-\frac{im}{2\hbar\tau}x^2\right)}{\left(1 + \frac{x^2}{\sigma^2}\right)^{\frac{1}{3}}} \left[1 + \tanh\left(\frac{x+x_b}{\sigma}\right)\right] \times \left[1 + \tanh\left(\frac{x-x_b}{\sigma}\right)\right], \quad (9)$$

where $x_b > 0$. The two smooth step functions represented by the hyperbolic tangents produce a relatively soft decay or cut-off at distance x_b/σ from the origin, which somehow mimics the effect of a limited aperture with soft boundaries, avoiding the appearance of spurious frequencies associated with a sudden cutoff or Gibbs phenomenon [29]. Because of the cutoff introduced, it is expected that there will not be time symmetry with respect to $t = \tau$, although the time-evolved of (9) will behave close to the exact solution.

We next perform a numerical integration of the evolution (2) using a standard pseudospectral method on a spatial mesh of size 50σ with a total of 1,024 grid points, integrating in time from $t = 0$ to $t = 2\tau$ with a time step $\delta t = 10^{-3}$, which suffices for our purposes. The numerical solution $\psi(x, t)$ is monitored through both density plots of the corresponding probability density and the associated quantum trajectories. A density plot of the probability density is shown in Fig. 2a), with a set of 51 trajectories (white solid lines) with equidistant initial conditions between $x/\sigma = -15$ and $x/\sigma = 15$ to cover a wide region of the initial probability density. We have chosen $x_b/\sigma = 22.5$.

As it can be noticed, as time approaches the critical value τ , the swarm of trajectories quickly evolves towards the origin, which turns into a prominent increase of the density within a very narrow spatial region, thus originating the singularity.

This behavior can be better appreciated in the zoomed version around the singular region displayed in Fig. 2a'). In the same manner, as time proceeds and becomes larger than τ , the swarm of trajectories gets dispersed quickly again. It is worth noting that, while the quantum flux is quite laminar before and after the singularity, as it is indicated by the relative smoothness of the trajectories (they evolve with nearly uniform motion), in the region around the singularity there is a turbulent flow led by the appearance of transient nodes. In their attempt for avoiding these nodes (nodal regions), the trajectories will be forced to undergo a whirling motion.

III. SINGULAR VERSUS SMOOTH WAVE PACKET EVOLUTION

To better understand the singularity, we will next examine a few characteristics of simpler but illustrative cases of smoothly

focusing wave packets.

A. Gaussian wave packet

As it is well known, the evolution of a Gaussian wave packet undergoes an initial boost or acceleration, and then it reaches a stationary linear expansion [30]. Consider the initial normalized Gaussian *ansatz*

$$\psi(x, 0) = \frac{1}{\sqrt{N_G}} \exp\left(-\frac{x^2}{4\sigma_0^2}\right), \quad (10)$$

where $\sigma_0 > 0$ is a real-valued parameter determining the width of the wave packet and the normalization constant is $N_G = \sqrt{2\pi\sigma_0^2}$. Substituting this into the free-space propagator leads to its time-evolved form,

$$\psi(x, t) = \frac{1}{\sqrt{N_G}} \sqrt{\frac{\sigma_0}{\tilde{\sigma}(t)}} \exp\left[-\frac{x^2}{4\sigma_0\tilde{\sigma}(t)}\right], \quad (11)$$

where the Gaussian complex-valued parameter

$$\tilde{\sigma}(t) = \sigma_0 \left(1 + \frac{i\hbar t}{2m\sigma_0^2}\right) \quad (12)$$

accounts for both the spreading in time of the wave packet, given by

$$\sigma(t) = |\tilde{\sigma}(t)| = \sigma_0 \sqrt{1 + \left(\frac{\hbar t}{2m\sigma_0^2}\right)^2}, \quad (13)$$

and the development of a space-dependent phase factor.

From the hydrodynamical point of view, the evolution of the above wave function maps onto the trajectories arising from the equation of motion

$$\dot{x} = \frac{\hbar^2 t}{(2m\sigma_0^2)^2} \frac{\sigma_0^2}{\sigma(t)^2} x. \quad (14)$$

After integration, this equation of motion renders the hyperbolic trajectories

$$x(t) = \frac{\sigma(t)}{\sigma_0} x(0). \quad (15)$$

From Eq. (14), it is clear that, for $t > 0$, the trajectories are “repelled” from the region where they are initially confined, namely, the waist of the wave packet, since the sign of \dot{x} directly depends on the sign of x and hence on the corresponding initial conditions. Although the initial expansion is slow, later on, for $t \gg t_s$, with $t_s = 2m\sigma_0^2/\hbar$ being a characteristic spreading time, it becomes essentially linear with time; for $t \sim t_s$, the expansion is accelerated, although at different rates as time proceeds [19].

All this information is nicely conveyed by the trajectories (15), which separate at a rate proportional to their initial

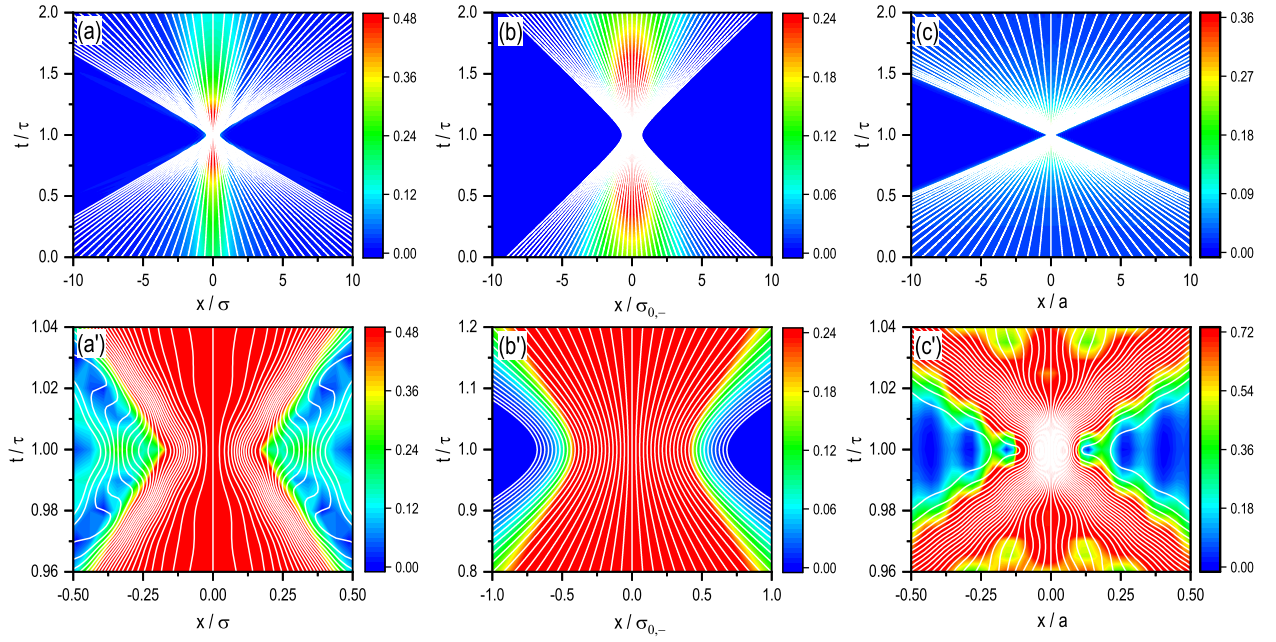


FIG. 2. (Top panels) Quantum trajectories (51) displayed on top of a density plot describing the time evolution of the probability associated with (a) the wave function (3) with $\nu = 1/3$, (b) the Gaussian (11) with waist width $\sigma_{0,-}$, and (c) the rectangular wave packet (19) with width a . For clarity in the density plot, due to the high values of the probability density around the singularity, it has been truncated to a tenth of its maximum value. (Bottom panels) Zoomed version of top panels around the focal region within the time interval where the maximum concentration of probability density is reached. The whirls in the trajectories denote the appearance and disappearance of nodes as the wave function approaches its maximum focusing.

distance, $d(0) = |x_2(0) - x_1(0)|$, since $d(t)/d(0) = \sigma(t)/\sigma_0$, where $d(t) = |x_2(t) - x_1(t)|$. Taking into account (13), for the same $d(0)$, the largest σ_0 , the slowest the dispersion, and vice versa, in compliance with what is expected in this case.

So far there are no novelties. However, we stress that the above solution is reversible in time, which means that, in the same way that the wave packet undergoes an expansion, it can also be tracked backwards. If the wave packet is then propagated ahead again, it will evolve imploding until reaching a minimum width (waist width), and then expanding again. Taking into account the translational time invariance of the solutions of the Schrödinger equation, if we call τ the time when waist occurs, we can define a generalized Gaussian coefficient as $\tilde{\sigma}_g(t) = \sigma(t - \tau)$. In this way the width and the phase of the wave packet at time t are given by

$$\begin{aligned} \sigma_g(t) &= \sigma_0 \sqrt{1 + \left[\frac{\hbar(t - \tau)}{2m\sigma_0^2} \right]^2}, \\ \theta_g(t) &= \arctan \left[\frac{\hbar(t - \tau)}{2m\sigma_0^2} \right]. \end{aligned} \quad (16)$$

It is clear from these expressions that, at $t = \tau$, we will observe a minimum waist, with $\sigma_g(\tau) = \sigma_0$, and zero phase, $\theta_g(\tau) = 0$.

Now, contrary to the standard case, we note that there are two factors ruling the expansion dynamics: one associated with the initial width and another one related to a phase, which play opposite roles. If σ_0 is too large, the phase factor decreases very rapidly, while a small width leads to a prominent phase

factor. This dependence is shown in Fig. 3, where the phase and modulus are separately represented for a better understanding. As it can be seen, $\sigma_g(0)$ has a minimum for $\sigma_0 = \sqrt{\tau/2}$, increasing linearly with σ_0 for large widths and as $1/\sigma_0$ when σ_0 goes to zero. The associated phase approaches $-\pi/2$ as σ_0 decreases, while tends to vanish rapidly as σ_0 increases above the threshold for minimum $\sigma_g(0)$.

From the above discussion, we may now consider the initial Gaussian ansatz as in (10), but replacing σ_0 with $\sigma_g(0)$. The associated time evolution can be directly obtained and leads to the trajectories

$$x(t) = \frac{\sigma_g(t)}{\sigma_0} x(0). \quad (17)$$

As before, these trajectories undergo an initial implosion, until $t = \tau$, and then a subsequent expansion. The question is how important the effect is, particularly taking into account that two different values of σ_0 , as it can readily be noticed from (16), can be associated with the same initial probability density. These two values will lead to very different dynamical behaviors. Thus, fixing the value of $\sigma_g(0)$, from (16) we obtain the following two admissible values for the waist width

$$\sigma_{0,\pm}^2 = \frac{1}{2} \sigma_g^2(0) \pm \sqrt{\sigma_g^4(0) - \left(\frac{\hbar\tau}{2m} \right)^2}. \quad (18)$$

To quantify the above effect, we consider a Gaussian wave packet with the (initial) width of its probability density at a

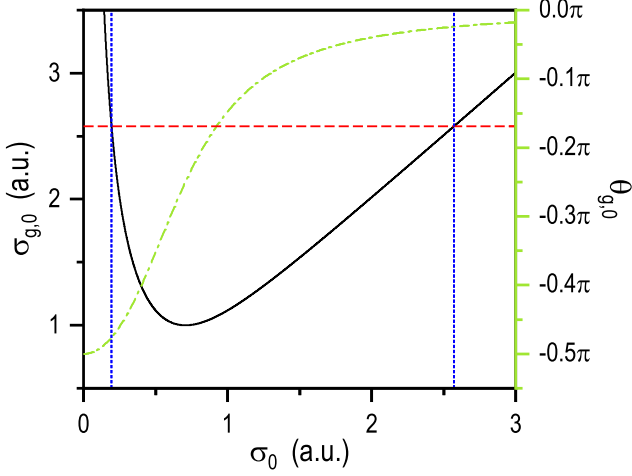


FIG. 3. Dependence of the phase (green line) and modulus (black line) of the initial complex-valued Gaussian parameter $\tilde{\sigma}_g$ on the waist width, σ_0 , for $t/\tau = 1$. The vertical blue dotted lines denote the values of the phase and modulus of $\tilde{\sigma}_c$ that correspond to Gaussians such that their width at 0.1 of their maximum value equals the same value of the probability density corresponding to the wave function. The horizontal red dashed line shows that there are always two Gaussian wave packets with the same initial width, but that lead to two different waist widths (in this case, $\sigma_g \approx 2.579$ is associated with $\sigma_{0,+} \approx 2.571$ and $\sigma_{0,-} \approx 0.194$). Despite having the same value for σ_g , each Gaussian wave packet has a very different initial phase, in particular, $\theta_{g,+} \approx -0.024\pi$ versus $\theta_{g,-} \approx -0.477\pi$.

tenth of the maximum value; i.e., $\varrho_G(s_{\pm}, 0)/\varrho_G(0, 0) = 0.1$, equal to the corresponding value for the (modified) singular wave function (9). This yields an initial width for both wave packets given by $\sigma_g^2(0) = (10\sqrt{10} - 1)/(2 \ln 10) \approx 6.6512$, which gives the waist widths $\sigma_{0,+} \approx 2.571$ and $\sigma_{0,-} \approx 0.194$. When compared with the value for $\sigma_g(0)$, we notice that while $\sigma_{0,+}$ is practically the same [$\sim 99\%$ $\sigma_g(0)$], which already indicates a poor dynamics, $\sigma_{0,-}$ is significantly different [$\sim 7.5\%$ $\sigma_g(0)$] and hence a more relevant dynamical behavior is expected.

The above expectations translate into the results displayed in Fig. 2b) for $\sigma_{0,-}$. The characteristic time scale here is $t_{s,-} \approx 0.15$, about a tenth of τ and hence with noticeable effects both in the implosion and, afterwards, in the subsequent dispersion. Note here that there is a more important phase contribution, since $\theta_{g,-}(0) \approx -0.38\pi$, a value closer to the maximum bound for the phase. Nonetheless, unlike the singular wave packet, here near the singular region the flux is not turbulent, which is consistent with the fact that the evolution of a Gaussian wave packet is characterized by the absence of nodes.

In Fig. 4 we plot the reverse case of a Gaussian wave packet for $\sigma_{0,+}$. We can appreciate that the wave packet remains unaffected, with the flux described by the swarm of 51 Bohmian trajectories being nearly stationary. The characteristic spreading time scale is $t_{s,+} \approx 26.4\tau$, which implies that neither the evolution before τ nor afterwards is going to be importantly affected. Indeed, the initial phase is $\theta_{g,+}(0) \approx -0.061\pi$, which already indicates the rather small contribution of the

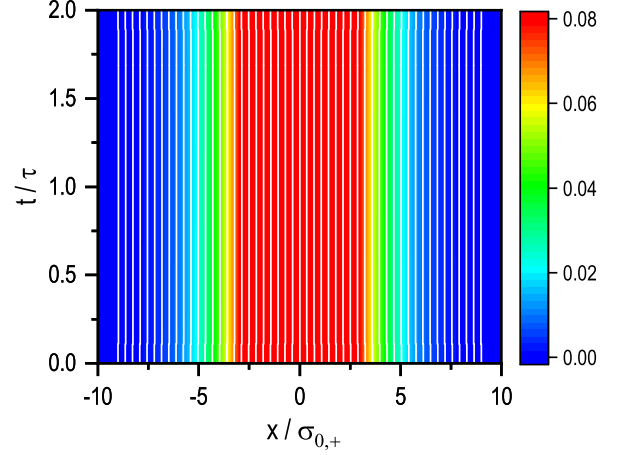


FIG. 4. Same trajectories as in Fig. 2b) for the probability associated with a Gaussian wave packet with waist width $\sigma_{0,+}$. Note that, because the waist width is relatively large compared to the initial width $\sigma_g(0)$, there is no apparent self-implosion (only a very slight narrowing at τ), as it is evidenced by the nearly parallel flux trajectories.

phase factor in the dynamics.

In Fig. 5 we represent the probability densities associated with these initial Gaussian wave packets. Interestingly, these probability densities are indistinguishable in position space, but they are completely different in momentum space: the momentum distribution for $\sigma_{0,+}$ is rather wide, while for $\sigma_{0,-}$ it approaches a Dirac delta function. It is precisely this wider momentum distribution that allows the second wave packet to coalesce toward the origin as the time approaches τ , similarly to the singular wave function, while the first wave packet will remain essentially the same.

B. Rectangular wave packet

As our last example, we consider a rectangular wave packet [31], with an initial profile

$$\psi(x, 0) = \frac{1}{\sqrt{N_r}} \exp\left(-\frac{im}{2\hbar\tau}x^2\right) \text{rect}_a(x), \quad (19)$$

where the rectangle function $\text{rect}_a(x)$ is defined as 1 for $|x| \leq a/2$ and 0 for $|x| > a/2$ and the normalization constant is $N_r = a$. The time evolution can be found using again (2), finding [31]

$$\psi(x, t) = \frac{(-1)^{3/4}}{\sqrt{4iN_r}} \exp\left(\frac{im}{2\hbar\tau}x^2\right) \left\{ \text{erfi}\left[(-1)^{1/4}\sqrt{\frac{m}{2\hbar t}}\left(x - \frac{a}{2}\right)\right] - \text{erfi}\left[(-1)^{1/4}\sqrt{\frac{m}{2\hbar t}}\left(x + \frac{a}{2}\right)\right] \right\}, \quad (20)$$

where $\text{erfi}(x)$ is the imaginary error function and this is valid for $t > 0$.

The wave packet is composed of an infinite number of plane waves. At time $t = 0$ these plane waves interfere to give

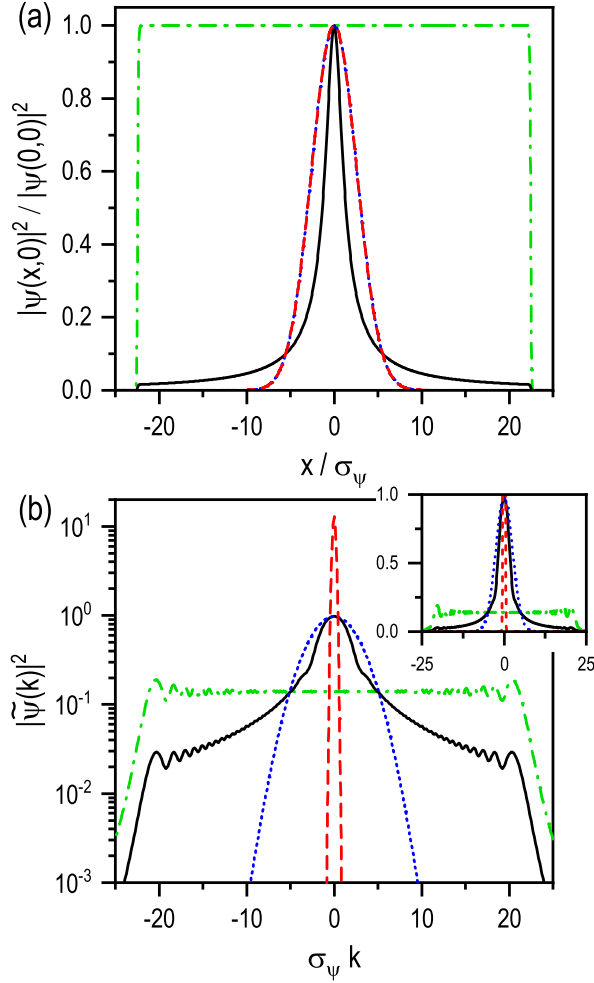


FIG. 5. Probability density in the x -position space (upper panel) and in the k -momentum space (lower panel) for the singular wave function (black solid line), a Gaussian wave packet with waist width $\sigma_{0,+}$ (red dashed line), and a Gaussian wave packet with waist width $\sigma_{0,-}$ (blue dotted line), and a rectangular wave packet (green dash-dotted line) for $t = 0$. The inset shows the same plots on a linear vertical scale. The waist widths for both Gaussians have been adjusted to the width of the probability density for the singular wave function at 0.1 of its maximum value.

a rectangular shape. As time elapses, the component plane waves travel, both to the right ($k > 0$) and to the left ($k < 0$), at different phase velocities $\hbar k/2m$. Thus the pattern of the interference of these plane waves gradually changes, resulting in the dispersion of the wave packet.

In Fig. 2c), we plot the quantum trajectories associated with this evolution. Near the time τ , we appreciate the presence of wiggles for both the singular and the rectangular wave packets, which remind of a nonlaminar flux. Conversely, the Gaussian profile looks perfectly laminar nearby the singular point. We recall that a flood in a river occurs because at some point water slows down and the quicker mass of water arriving from behind finds this “potential barrier” created by the slow water and tries to overcome it. In this case, the wiggles mark somehow a *slower light flow*, so that energy accumulates nearby the

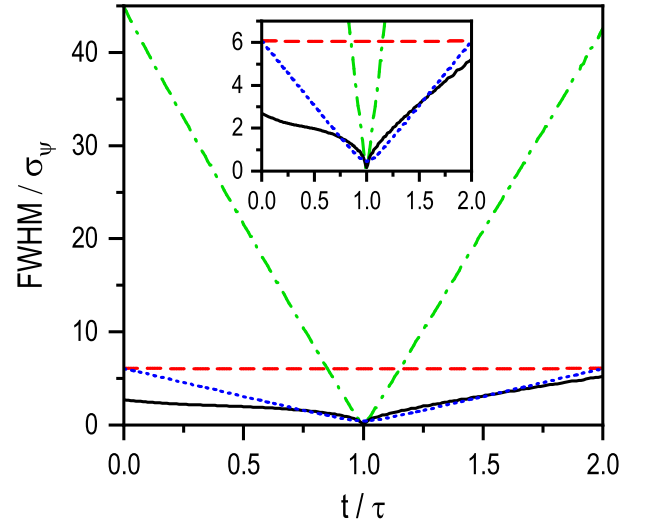


FIG. 6. Evolution temporal of the FWHM for the same wave packets as in Fig. 5, with the same symbols: the singular wave function (black solid line), a Gaussian wave packet with waist width $\sigma_{0,+}$ (red dashed line), a Gaussian wave packet with waist width $\sigma_{0,-}$ (blue dotted line), and a rectangular wave packet (green dash-dotted line).

singularity and the density grows.

An alternative way to capture the degree of localization of a wave function is by studying the behavior exhibited its full width at half maximum (FWHM) [32]. More specifically, this quantity is computed in all cases determining the distance between the two positions, x_+ and x_- , at which the corresponding probability density reaches half its maximum value at any time; that is

$$\frac{\varrho(x_{\pm}, t)}{\varrho_{\max}(x, t)} = \frac{1}{2}. \quad (21)$$

Except for Gaussian wave packets, the above equation cannot be solved analytically, so x_+ and x_- have been numerically determined on the fly, during the time-evolution of the corresponding wave functions. From this, we obtain $\text{FWHM}(t) = x_+(t) - x_-(t)$, which is shown in Fig. 6 for the for cases here considered. As it can be noticed, while the FWHM is nearly constant for the Gaussian with waist width $\sigma_{0,+}$, it shows a linear decrease and increase, before and after the waist, respectively, for the Gaussian with $\sigma_{0,-}$. A similar trend is also observed for the square wave function, although the FWHM shows a tiny asymmetry before and after the singularity, which is related to the limitations involved in the numerical method (the spatial size of the grid sets a cutoff for the high spatial frequencies). Finally, for the singular wave function (3), the FWHM slowly decrease until t is close to τ , as it can be appreciated in the inset of Fig. 6. Near this time, the FWHM undergoes a sudden decrease and then increase afterwards; at any later time, the FWHM increase near linearly, in a similar fashion to the Gaussian with $\sigma_{0,-}$. We notice again a different behavior between the FWHM dynamics before and after $t = \tau$, which is related to the fact that the wave function considered is not exactly the ansatz $\text{eqref{psi0}}$, but

the truncated version (9). All these characteristics concur with the corresponding probability density and quantum trajectories displayed in Fig. 2.

IV. CONCLUDING REMARKS

To summarize, we have studied a family of solutions of the Schrödinger equation that spontaneously develop a singularity while propagating in free space. Due to the finiteness of these solutions, their singularities do not require a nonphysical infinite amount of energy to manifest. Nevertheless, the local amplitude of the field at a singular point may grow unboundedly. We have given a physical interpretation in terms of quantum trajectories.

While there is a widespread belief that extreme focusing requires strong nonlinear effects, we have demonstrated that this can be easily achieved with only linear propagation. This promising field enhancement mechanism may foster further interesting research in fields such as electron microscopy or optics.

ACKNOWLEDGMENTS

Financial support is acknowledged to the Spanish Research Agency (Grant No. PID2021-127781NB-I00). AA acknowledges support from Deutsche Forschungsgemeinschaft (Grant No. 429529648-TRR 306).

-
- [1] T. Tao, *Nonlinear dispersive equations. Local and global analysis*, CBMS Regional Conference Series in Mathematics, Vol. 106 (AMS, Providence, RI, 2006).
 - [2] W. Schlag, *Mathematical aspects on nonlinear dispersive equations* (Princeton University Press, Princeton, 2007).
 - [3] R. Mandel, Dispersive estimates, blow-up and failure of strichartz estimates for the schrödinger equation with slowly decaying initial data, *Pure Appl. Anal.* **2**, 519 (2020).
 - [4] C. Dietze, Dispersive estimates for nonlinear Schrödinger equations with external potentials, *J. Math. Phys.* **62**, 111502 (2021).
 - [5] A. Peres, *Quantum Theory: Concepts and Methods* (Kluwer, New York, 2002).
 - [6] J. L. Bona and J.-C. Saut, Dispersive blow-up II. Schrödinger-type equations, optical and oceanic rogue waves, *Chin. Ann. Math. Ser. B* **31**, 793 (2010).
 - [7] C. Sulem and P. L. Sulem, *The Nonlinear Schrödinger Equation: Self-Focusing and Wave Collapse* (Springer, New York, 1999).
 - [8] G. Fibich, *The Nonlinear Schrödinger Equation: Singular Solutions and Optical Collapse* (Springer, Cham, 2015).
 - [9] N. Karjanto, Understanding the Schrödinger Equation: Some [Non]Linear Perspectives (Nova, New York, 2020) Chap. The Nonlinear Schrödinger Equation: A Mathematical Model with Its Wide Range of Applications.
 - [10] L. Hörmander, Estimates for translation invariant operators in L^p spaces, *Acta Math.* **104**, 93 (1960).
 - [11] A. Aiello, Spontaneous generation of singularities in paraxial optical fields, *Opt. Lett.* **41**, 1668 (2016).
 - [12] A. Aiello, M. Paúr, B. Stoklasa, Z. Hradil, J. Řeháček, and L. L. Sánchez-Soto, Observation of concentrating paraxial beams, *OSA Continuum* **3**, 2387 (2020).
 - [13] M. A. Porras, Exploding paraxial beams, vortex beams, and cylindrical beams of light with finite power in linear media, and their enhanced longitudinal field, *Phys. Rev. A* **103**, 033506 (2021).
 - [14] G. Nienhuis, Analogies between optical and quantum mechanical angular momentum, *Philos. Trans. R. Soc. A* **375**, 20150443 (2017).
 - [15] D. Bohm, A suggested interpretation of the quantum theory in terms of “hidden” variables. I, *Phys. Rev.* **85**, 166 (1952).
 - [16] D. Bohm, A suggested interpretation of the quantum theory in terms of “hidden” variables. II, *Phys. Rev.* **85**, 180 (1952).
 - [17] D. Bohm and B. J. Hiley, *The Undivided Universe* (Routledge, New York, 1993).
 - [18] B.-G. Englert, M. O. Scully, G. Süssmann, and H. Walther, Surrealistic Bohm trajectories, *Z. Naturforsch. A* **47**, 1175 (1993).
 - [19] A. S. Sanz and S. Miret-Artés, Quantum phase analysis with quantum trajectories: A step towards the creation of a bohmian thinking, *Am. J. Phys.* **80**, 525 (2012).
 - [20] D. H. Mahler, L. Rozema, K. Fisher, L. Vermeyden, K. J. Resch, H. M. Wiseman, and A. Steinberg, Experimental nonlocal and surreal Bohmian trajectories, *Sci. Adv.* **2**, e1501466 (2016).
 - [21] A. S. Sanz, Bohm’s approach to quantum mechanics: Alternative theory or practical picture?, *Front. Phys.* **14**, 11301 (2019).
 - [22] E. Merzbacher, *Quantum Mechanics*, 3rd ed. (Wiley, New York, 1998).
 - [23] R. J. Iorio and V. M. Iorio, *Fourier Analysis and Partial Differential Equations* (Cambridge University Press, Cambridge, 2001).
 - [24] N. Aronszajn and K. T. Smith, Theory of Bessel potentials. I, *Ann. Inst. Fourier* **11**, 385 (1961).
 - [25] DLMF, *NIST Digital Library of Mathematical Functions*, <http://dlmf.nist.gov/>, Release 1.1.8 of 2022-12-15, f. W. J. Olver, A. B. Olde Daalhuis, D. W. Lozier, B. I. Schneider, R. F. Boisvert, C. W. Clark, B. R. Miller, B. V. Saunders, H. S. Cohl, and M. A. McClain, eds.
 - [26] P. R. Holland, *The Quantum Theory of Motion* (Cambridge University Press, Cambridge, 1993).
 - [27] L. I. Schiff, *Quantum Mechanics*, 3rd ed. (McGraw-Hill, Singapore, 1968).
 - [28] A. S. Sanz, Bohm’s quantum “non-mechanics”: An alternative quantum theory with its own ontology?, *Ann. Fond. Louis Broglie* **46**, 19 (2021).
 - [29] E. Hewitt and R. E. Hewitt, The Gibbs-Wilbraham phenomenon: An episode in Fourier analysis, *Arch. Hist. Exact Sci.* **21**, 129 (1979).
 - [30] A. S. Sanz and S. Miret-Artés, *A Trajectory Description of Quantum Processes. II. Applications*, Lecture Notes in Physics, Vol. 831 (Springer, Berlin, 2014).
 - [31] K. Mita, Dispersion of non-Gaussian free particle wave packets, *Am. J. Phys.* **75**, 950 (2007).
 - [32] A. García-Sánchez and A. S. Sanz, Analysis of the gradual transition from the near to the far field in single-slit diffraction, *Phys. Scr.* **97**, 055507 (2022).